NANO LETTERS
Cite This: Nano Lett. 2018, 18, 2937−2942
Letter
pubs.acs.org/NanoLett

The Pentagonal Nature of Self-Assembled Silicon Chains and Magic Clusters on Ag(110)

Shaoxiang Sheng,[†,∥,#] Runze Ma,[‡,#] Jiang-bin Wu,[§,∥,#] Wenbin Li,[†,∥] Longjuan Kong,[†,∥] Xin Cong,[§,∥] Duanyun Cao,[‡] Wenqi Hu,[†,∥] Jian Gou,[†,∥] Jun-Wei Luo,[§,∥] Peng Cheng,[†,∥] Ping-Heng Tan,[*,§,∥,∞] Ying Jiang,[*,‡,⊥,∞] Lan Chen,[†,∥] and Kehui Wu[*,†,∥,⊥,∞]

[†]Institute of Physics, Chinese Academy of Sciences, Beijing 100190, China

[‡]International Center for Quantum Materials, School of Physics, Peking University, Beijing 100871, China

[§]State Key Laboratory of Superlattices and Microstructures, Institute of Semiconductors, Chinese Academy of Sciences, Beijing 100083, China

[∥]School of Physics, and College of Materials Science and Optoelectronic Technology, University of Chinese Academy of Sciences, Beijing 100049, China

[⊥]Collaborative Innovation Center of Quantum Matter, Beijing 100871, China

[∞]CAS Center for Excellence in Topological Computation, University of Chinese Academy of Sciences, Beijing 100190, China

S *Supporting Information*

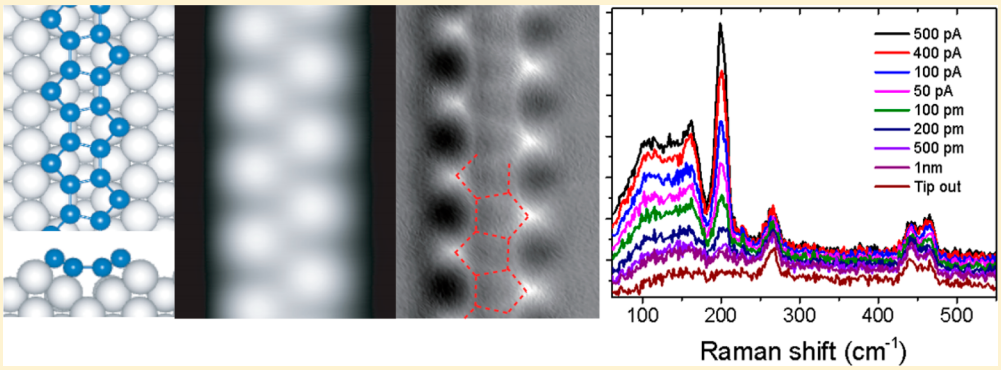

ABSTRACT: The atomic structures of self-assembled silicon nanoribbons and magic clusters on Ag(110) substrate have been studied by high-resolution noncontact atomic force microscopy (nc-AFM) and tip-enhanced Raman spectroscopy (TERS). Pentagon-ring structures in Si nanoribbons and clusters have been directly visualized. Moreover, the vibrational fingerprints of individual Si nanoribbon and cluster retrieved by subnanometer resolution TERS confirm the pentagonal nature of both Si nanoribbons and clusters. This work demonstrates that Si pentagon can be an important element in building silicon nanostructures, which may find important applications for future nanoelectronic devices based on silicon.

KEYWORDS: *Noncontact atomic force microscopy (nc-AFM), tip-enhanced Raman spectroscopy (TERS), pentagon silicon chains, magic cluster*

Pentagon is one of the most beautiful geometric structures in nature, but it is rarely seen in crystals because 5-fold symmetry is mathematically forbidden in a two-dimensional (2D) or 3D periodic lattices. Fortunately, a pentagon can be an elementary building block in 1D or 0D systems because translational symmetry is not required there. For example, pentagons can often be found in low-dimensional carbon systems, such as the Stone−Wales defects at the boundaries of graphene,[1−3] in carbon nanotube,[4] or in fullerene molecules.[5,6] However, in these systems pentagons only compose a small portion of the structure. So far, 1D or 0D systems consisting of purely pentagons are still rare.

It has been known that on anisotropic Ag(110) surface, silicon atoms spontaneously form 1D nanoribbons (SiNRs) aligned along the [$\bar{1}$10] direction of Ag(110) substrate, as was first reported by Leandri et al.[7] The atomic structure of the SiNRs, however, has remained controversial. More than 10 structure models have been proposed in literature, including chainlike mode, hexagonal silicene model, and Ag−Si alloy model.[8−16] Remarkably, a recent model proposed by Cerdá et al. suggested that the SiNRs are composed of purely silicon

Received: January 21, 2018
Revised: March 20, 2018
Published: March 30, 2018

DOI: 10.1021/acs.nanolett.8b00289
Nano Lett. 2018, 18, 2937−2942

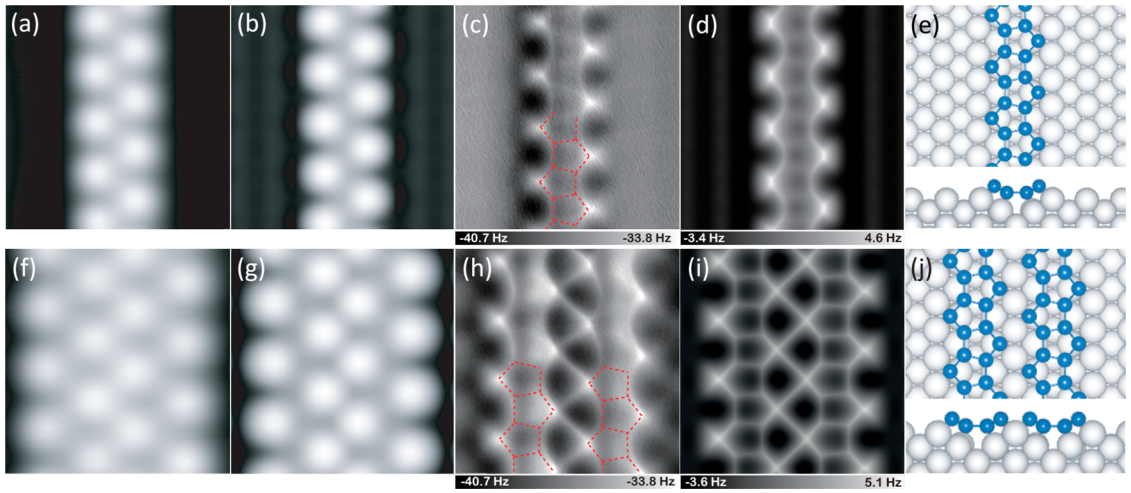

Figure 1. Si SNR and DNR on Ag(110) surface. (a,b) Experimental and simulated STM images of Si SNR, respectively. (c,d) Experimental and simulated nc-AFM images of Si SNR, respectively. (e) Atomic structure of the SNR on Ag(110) in top and side views. Ag, Si atoms are denoted as white and blue spheres, respectively. (f–i) STM (f) and AFM (h) images of Si DNR and the corresponding simulated ones (g,i). (j) Atomic structure of the DNR on Ag(110) in top and side views. Set point of STM images for (a,f) are V = 100 mV and I = 20 pA. The tip height of experimental (simulated) AFM images in (c,d,h,i) are −150 pm (8.91 Å) and −200 pm (8.91 Å), respectively. The tip height of experimental AFM images is referenced to the STM set point on the Ag surface next to the NRs (100 mV, 50 pA). The oscillation amplitudes of experimental images are 100 pm. All the AFM simulations were done with a quadrupole (d_z^2) tip (k = 0.5 N/m, Q = 0.0 e).

pentagons,[17] which was supported by a following experiment based on grazing incidence X-ray diffraction (GIXD).[18] However, because scanning tunneling microscopy (STM) reflects surface electronic states instead of the exact atomic geometry, and GIXD is a macro-probe method, this model still largely relied on theoretical modeling and cannot completely rule out other possibilities.

In this Letter, we provide two forms of solid experimental evidence that the SiNRs on Ag(110) is composed of purely Si pentagons. First, by using noncontact atomic force microscopy (nc-AFM) with the tip decorated by a CO molecule, we were able to visualize the Si pentagon rings directly. Second, by using tip-enhanced Raman spectroscopy (TERS), we were able to retrieve the local vibrational fingerprint of SiNRs, which fits perfectly to the Si pentagon model rather a hexagon model. These two experiments unambiguously pin-down the pentagonal nature of the SiNRs. Moreover, we have achieved single-cluster TERS spectrum for Si magic clusters that coexist with SiNRs on Ag(110) surface at low Si coverage. In contrast to the so-far proposed hexagonal model for Si magic clusters,[17] our results based on both nc-AFM and TERS revealed that they are composed of a pair of Si pentamers. This work demonstrates that Si pentagon can be an important element in building silicon nanostructures, which may be important for future nanoelectronic devices based on silicon.

Experimental Section. The Si NRs were grown in a ultrahigh vacuum system (based pressure <10^{-10} Torr) by deposition of Si to a clean Ag(110) substrate with a piece of Si wafer heated to about 1300 K. The STM and AFM images were performed with a STM/nc-AFM system (Createc, Germany) at 5 K using a qPlus sensor equipped with a W tip (spring constant $k_0 \approx$ 1800 N/m, resonance frequency f_0 = 26.7 kHz, and quality factor $Q \approx$ 60000). A CO molecule was attached to the tip for high-resolution AFM imaging.[19] The methods for first-principles calculations and STM/AFM image simulations were included in Supporting Information.[20−26] The TERS experiment were carried out in a homemade LT-UHV-STM based TERS system at 77 K and with a base pressure about 2 × 10^{-10} mbar. Chemically etched Ag tips were used for STM imaging and TERS measurements. A p-polarized laser with wavelength at 532 nm was used as pump source for Raman measurement, and the polarization is along the tip axis for TERS experiments.[27]

Results and Discussion. At room temperature, Si nanoribbons formed on Ag(110) surface consists of a single-strand (SNRs, 0.8 nm in width). Upon annealing at about 460 K, most ribbons are converted to double-strand ones (DNRs, 1.6 nm in width). Figure 1a shows a typical STM image of Si SNRs, which features a 2× superstructure with respect to the Ag(110) substrate. The image is consistent with previous reports and the simulated STM image with the pentagon model (Figure 1b). However, it is beyond the capability of STM to resolve a finer structure other than the zigzag protrusions along the chain. In contrast, the simultaneously obtained high resolution nc-AFM image of SNR, as shown in Figure 1c, gives clearly more details of the structure. Pentagonal rings aligned in a zigzag manner along the chain can be directly visualized, as outlined by red dash lines as a guide to the eyes. We notice that the pentagons are slightly distorted, probably due to the inhomogeneous relaxation of the CO molecule at the tip apex during the scanning.[28]

It is worth to note that in the pentagon structural model, a row of Ag atoms underneath the Si SNRs is missing. Accordingly, in each Si pentagon four inner Si atoms are laying in the missing-silver trough, and the one at the outer corner is located on a silver bridge site (Figure 1e). This corner Si atom is thus slightly buckled up by 70 pm.[17] This structural feature perfectly explains the relatively bright outer corner of the Si pentagon observed in nc-AFM images. Figure 1d shows the simulated AFM image of the Si SNR with the pentagon model, which fits the experiment very well.

Similarly, the experimental and simulated STM images of a double-strand ribbon (DNR) are shown in Figure 1f,g. For the DNRs, the nc-AFM image (Figure 1h) shows many spiral, interconnecting bright lines between two NRs. This feature is perfectly reproduced by the simulated AFM image (Figure 1i)

DOI: 10.1021/acs.nanolett.8b00289
Nano Lett. 2018, 18, 2937−2942

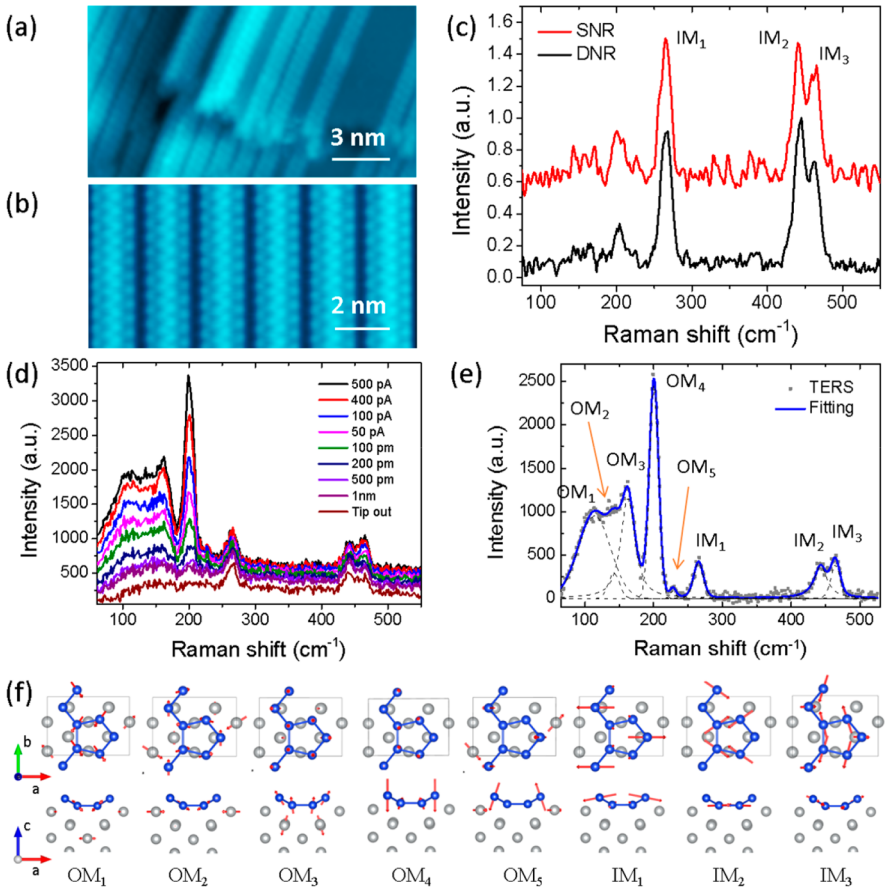

Figure 2. Normal Raman and TERS spectra of Si NRs. (a,b) STM images of SNRs (a) and DNRs (b) grown at room temperature and 460 K, respectively. (c) The corresponding normal Raman spectra of SNRs (300 s) and DNRs (600 s) in (a,b). (d) Gap-distance dependent TERS spectra of SNRs (1 V). (e) TERS spectrum of SNRs, experimental data are shown by gray crosses, and the fitting data are plotted by blue solid line. (f) The atomic vibration schematics of each Raman mode with top and side views.

based on the pentagon model (Figure 1j). The interconnecting lines should not be automatically related to presence of interatomic bonds, instead they represent ridges of the potential energy landscape experienced by the functionalized probe.[24,29]

Raman spectroscopy provides vibrational information on chemical bonds, which serves as chemical fingerprints of molecules. Raman spectrum of DNRs has been measured with 488 nm excitation laser previously,[30] however, the Raman spectrum of SNRs has not been reported so far. We performed Raman spectroscopy (without tip enhancement) measurements of both SNRs and DNRs. In this case, we prepared two samples with dominating SNRs and DNRs, respectively, by controlling the sample temperature, as shown in Figure 2a,b. Note that a long Raman spectrum accumulation time is necessary in order to obtain a reasonable signal-to-noise ratio. The Raman spectra of SNRs and DNRs, as shown in Figure 2c, are almost identical to each other. This indicates that their atomic structures are the same, with no chemical bonds between the two strands of Si atoms in DNRs (Figure 1j). There are three major peaks at about 265, 440, and 465 cm^{-1} and two weak peaks at 165 and 201 cm^{-1}. These peaks are completely different from the vibrational frequencies predicted base on a hexagonal model of Si NRs.[31] Remarkably, we calculated the vibrational frequencies based on the pentagon model of Si SNRs, and they match with the experimental ones very well, as details discussed later. Therefore, our Raman data provides another solid evidence that the Si NRs is composed of pentagonal Si rings instead of hexagonal rings. The possibility of surface alloying can also be ruled out because it will cause significantly different phonon spectrum.

In additional to normal Raman, we further performed tip-enhanced Raman spectroscopy (TERS) to clarify the nature of the vibrational modes. First reported in 2000,[32] TERS with single molecule sensitivity and ultrahigh spatial resolution has developed into a optical nanoimaging method.[33−35] We have utilized TERS to identify different silicene phases which differ only in their Si−Si bond directions on Ag(111) surface.[27] The selective enhancement of Raman modes by TERS provides critical information for identifying the origination of Raman modes. As shown in Figure 2d, the gap-distance-dependent TERS spectra of SNRs shows that the intensity of the OM_1 to OM_4 peaks, which are below 200 cm^{-1}, are strongly enhanced in gap-mode TERS and become the dominant peaks at small tip−sample distance. In contrast, the three major Raman peaks (IM_1, IM_2, and IM_3) get very little enhancement and becomes insignificant. Only the IM_3 peak is slightly enhanced and becomes stronger than the IM_2 peak. This selective enhancement behavior can be perfectly explained by the vibrational schematics as shown in Figure 2f. As we know, TERS mainly enhances the vibration modes which contains out-of-plane vibration components, that is, model with nonzero α_{zz} component in the Raman tensor.[27,33] As illustrated in Figure 2f, the low energy modes (OM_1 to OM_5) all have significant

DOI: 10.1021/acs.nanolett.8b00289
Nano Lett. 2018, 18, 2937−2942

vertical components, agreeing with their significant enhancement in TERS. The high energy IM_3 also contains a clear vertical component although not as large as the low energy modes. In contrast, the IM_1 and IM_2 modes have almost purely in-plane vibrations, and therefore they exhibit negligible enhancement. We shall emphasize that in the normal Raman spectra, the low frequency modes are too week to perform a reliable analysis, while in TERS they are clearly unveiled and can be reliably analyzed. As summarized in Table 1, the calculated Raman frequencies match exactly with the experimental results, this shows that TERS is a powerful tool to study the vibrational properties of low-dimensional materials.

Table 1. Calculated Vibrational Modes and Corresponding Frequencies of the Pentagon Model of Si SNRs

modes	exp (cm^{-1})	theo (cm^{-1})	diff. (cm^{-1})
IM_3	464	457	7
IM_2	442	440	2
IM_1	265	269	−4
OM_5	228	233	−5
OM_4	201	208	−7
OM_3	163	164	−1
OM_2	143	145	−2
OM_1	115	110	5

Furthermore, high-resolution TERS spectra obtained in individual SNRs and DNRs are almost identical (see Supporting Information Figure S1), further confirming that there is no chemical bond formation between the two strands of the DNR. Nevertheless, the repulsive interaction between them can result in a slight compression of the Si−Si bonds (~0.001 Å), as can be revealed by the highly sensitive blue shift of the TERS peaks.[36]

Finally, we studied Si magic clusters on Ag(110), which are very important for studying the origin of pentagon rings in SiNRs. The clusters coexist with SNRs at room temperature and low coverage.[17,37] All clusters appear identical in the STM images with a pair of bright spots in the center and two darker wings at both sides (Figure 3a,f,g). These magic clusters are considered to be the precursor for self-assembly of SNRs. In ref 17, Cerdá et al. proposed a model with a hexagonal Si ring and 4 Si adatoms. On the basis of this assumption, they suggested a transition from hexagon to pentagon structure during the formation of SNRs. Here, we show by nc-AFM and TERS experiments that it is not the case. First, the extremely high sensitive and spatial resolution of our TERS allow us to obtain for the first time single-cluster Raman spectrum, as shown in Figure 3b. One major Raman peak is observed at 203 cm^{-1} when the tip is on the top of the cluster, as indicated by the Raman intensity profile of the mode at 203 cm^{-1} (Figure 3c). This profile was measured along the line in the inset STM image in Figure 3b, in agreement with the topography height profile of the cluster, confirming the extremely high spatial resolution of our TERS system. The 203 cm^{-1} peak is almost identical to the OM_4 peak of the SNRs and differs completely from the calculated results for a hexagonal Si ring with adatoms, whose out-of-plane modes is at 143 cm^{-1} (Figure S2c in the Supporting Information). In order to explain our data, we proposed a structural model containing two Si pentagons sitting side by side, with four Si adatoms attached to the edge (Figure 3e). In addition, it should be noted that the cluster model is placed on a Ag divacancy. This structure is similar to the pentagon chain model of the SNR, and the calculation indeed gives a main out-of-plane vibrational mode at 207 cm^{-1} (Figure 3d), consistent with the experiments very well.

To further confirm the cluster structure, high-resolution nc-AFM image was also obtained, as shown in Figure 3h. The detailed features of the image fitted perfectly the simulated

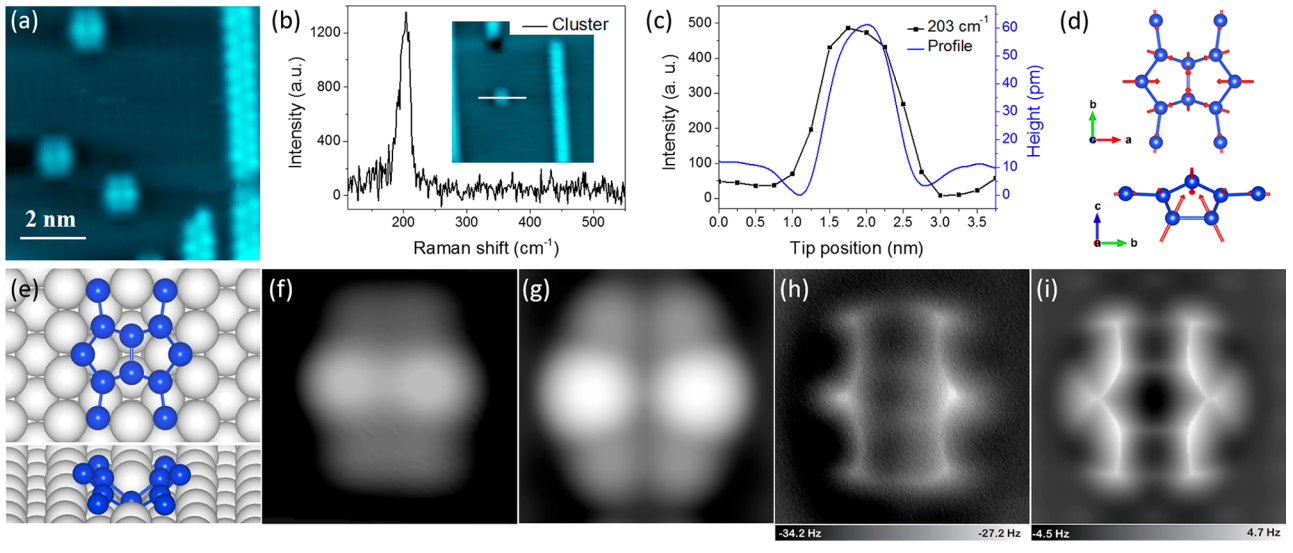

Figure 3. TERS spectrum and atomic structure of Si nanocluster. (a) STM of the Si cluster and SNRs at low Si coverage (1 V, 50 pA). (b) TERS spectrum of the cluster in the inset STM image. (c) TERS intensity profile of the 203 cm^{-1} mode along the line in (b) with an interval of 0.25 nm every step, and the STM topography height profile (blue line). (d) Atomic vibration schematic of the 203 cm^{-1} mode of the cluster. (e) Atomic structure of the Si cluster on a Ag divacancy Ag(110) surface, with top and perspective views. (f) High-resolution STM images of the cluster (100 mV, 50 pA). (g) Simulated STM image of the cluster (1 V). (h) Corresponding AFM image of the cluster in (f). The tip height of experimental AFM image is −170 pm, which is referenced to the STM set point on the Ag surface next to the nanocluster (100 mV, 50 pA). (i) Simulated AFM image of the cluster. The tip height in simulations is 9.21 Å, defined as the vertical distance between the apex atom of the metal tip and the highest Ag atom of the substrate. All the oscillation amplitudes of experimental and simulated images are 100 pm.

DOI: 10.1021/acs.nanolett.8b00289
Nano Lett. 2018, 18, 2937−2942

AFM image of the pentagon structure (Figure 3i), instead of the hexagon one (Figure S2b in the Supporting Information). We note that the pentagon structures cannot be easily distinguished in both the experimental and simulated AFM images. This is due to the highly buckling nature of the Si cluster, where the central two Si atoms are located deeply in the Ag divacancy (Figure 3e). Actually, we found that when more Ag atoms underneath the cluster are removed from the surface to form a trough as in the SNR case, the cluster structure becomes unstable and spontaneously transfer into the NRs structure. Thus, this model can explain the dynamics transition from cluster precursor to NRs as well.

In conclusion, our state-of-the-art nc-AFM and TERS experiments provide solid evidence, including the direct visualization and vibrational fingerprints, that Si NRs were composed of purely pentagon rings. Furthermore, the structure of the Si magic cluster was found to contain also pentagonal Si rings in contrast to previously proposed hexagonal rings. We note that Si NRs possesses intriguing properties, such as strong resistance to oxidation[38] and interesting 1D transport characteristics.[9,37] Hydrogenated Si NRs may possess peculiar magnetic properties such as ferromagnetic or antiferromagnetic.[39] These properties based on pentagonal Si rings are not only fundamentally important but also potentially applicable in nanoelectronic and spintronic applications involving low-dimensional silicon structures.

■ ASSOCIATED CONTENT

Supporting Information

The Supporting Information is available free of charge on the ACS Publications website at DOI: 10.1021/acs.nanolett.8b00289.

Detailed methods of the first-principles structure calculations and the simulation of the nc-AFM images. Some fine differences between the TERS spectra of SNR and DNR. Additional discussion on the structure model of the Si clusters (PDF)

■ AUTHOR INFORMATION

Corresponding Authors

*E-mail: phtan@semi.ac.cn.
*E-mail: yjiang@pku.edu.cn.
*E-mail: khwu@iphy.ac.cn.

ORCID

Ping-Heng Tan: 0000-0001-6575-1516
Kehui Wu: 0000-0002-7698-5673

Author Contributions

#S.S., R.M., and J.-b.W. contributed equally to this work.

Notes

The authors declare no competing financial interest.

■ ACKNOWLEDGMENTS

This work was supported by the National Key R&D Program under Grants 2016YFA0300904, 2016YFA0301204, and the National Natural Science Foundation of China under Grants 11334011, 11474277, 11434010, and the Key Research Program of the Chinese Academy of Sciences under Grants no. XDB07010200, XDPB06, XDPB08. Y.J. acknowledges support by National Science Fund for Distinguished Young Scholars and Cheung Kong Young Scholar Program.

■ REFERENCES

(1) Huang, P. Y.; Ruiz-Vargas, C. S.; van der Zande, A. M.; Whitney, W. S.; Levendorf, M. P.; Kevek, J. W.; Garg, S.; Alden, J. S.; Hustedt, C. J.; Zhu, Y.; Park, J.; McEuen, P. L.; Muller, D. A. *Nature* **2011**, *469*, 389−92.
(2) Jia, X.; Campos-Delgado, J.; Terrones, M.; Meunier, V.; Dresselhaus, M. S. *Nanoscale* **2011**, *3*, 86−95.
(3) Girit, C. O.; Meyer, J. C.; Erni, R.; Rossell, M. D.; Kisielowski, C.; Yang, L.; Park, C. H.; Crommie, M. F.; Cohen, M. L.; Louie, S. G.; Zettl, A. *Science* **2009**, *323*, 1705−1708.
(4) Suenaga, K.; Wakabayashi, H.; Koshino, M.; Sato, Y.; Urita, K.; Iijima, S. *Nat. Nanotechnol.* **2007**, *2*, 358−60.
(5) Kroto, H. W.; Heath, J. R.; O'brien, S. C.; Curl, R. F.; Smalley, R. E. *Nature* **1985**, *318*, 162−163.
(6) Kroto, H. W. *Nature* **1987**, *329*, 529−531.
(7) Leandri, C.; Lay, G. L.; Aufray, B.; Girardeaux, C.; Avila, J.; Dávila, M. E.; Asensio, M. C.; Ottaviani, C.; Cricenti, A. *Surf. Sci.* **2005**, *574*, L9−L15.
(8) Aufray, B.; Ealet, B.; Jamgotchian, H.; Maradj, H.; Hoarau, J.-Y.; Biberian, J.-P. Growth of Silicon Nano-ribbons on Ag(110): State of the Art. In *Silicene: Structures, Properties and Applications*; Michelle, S.; Tetsuya, M., Eds.; Springer International Publishing, 2016; Vol. *235*, pp 183−202.
(9) Feng, B.; Li, H.; Meng, S.; Chen, L.; Wu, K. *Surf. Sci.* **2016**, *645*, 74−79.
(10) Hogan, C.; Colonna, S.; Flammini, R.; Cricenti, A.; Ronci, F. *Phys. Rev. B: Condens. Matter Mater. Phys.* **2015**, *92*, 115439.
(11) Colonna, S.; Serrano, G.; Gori, P.; Cricenti, A.; Ronci, F. *J. Phys.: Condens. Matter* **2013**, *25*, 315301.
(12) Lian, C.; Ni, J. *Phys. B* **2012**, *407*, 4695−4699.
(13) Aufray, B.; Kara, A.; Vizzini, S. b.; Oughaddou, H.; Léandri, C.; Ealet, B.; Le Lay, G. *Appl. Phys. Lett.* **2010**, *96*, 183102.
(14) Sahaf, H.; Léandri, C.; Moyen, E.; Macé, M.; Masson, L.; Hanbücken, M. *Europhys. Lett.* **2009**, *86*, 28006.
(15) De Padova, P.; Quaresima, C.; Perfetti, P.; Olivieri, B.; Leandri, C.; Aufray, B.; Vizzini, S.; Le Lay, G. *Nano Lett.* **2008**, *8*, 271−275.
(16) He, G. M. *Phys. Rev. B: Condens. Matter Mater. Phys.* **2006**, *73*, 035311.
(17) Cerda, J. I.; Slawinska, J.; Le Lay, G.; Marele, A. C.; Gomez-Rodriguez, J. M.; Davila, M. E. *Nat. Commun.* **2016**, *7*, 13076.
(18) Prévot, G.; Hogan, C.; Leoni, T.; Bernard, R.; Moyen, E.; Masson, L. *Phys. Rev. Lett.* **2016**, *117*, 276102.
(19) Gross, L.; Mohn, F.; Moll, N.; Liljeroth, P.; Meyer, G. *Science* **2009**, *325*, 1110−1114.
(20) Baroni, S.; de Gironcoli, S.; Dal Corso, A.; Giannozzi, P. *Rev. Mod. Phys.* **2001**, *73*, 515−562.
(21) Kresse, G.; Joubert, D. *Phys. Rev. B: Condens. Matter Mater. Phys.* **1999**, *59*, 1758−1775.
(22) Kresse, G.; Furthmuller, J. *Phys. Rev. B: Condens. Matter Mater. Phys.* **1996**, *54*, 11169−11186.
(23) Blöchl, P. E. *Phys. Rev. B: Condens. Matter Mater. Phys.* **1994**, *50*, 17953−17979.
(24) Hapala, P.; Kichin, G.; Wagner, C.; Tautz, F. S.; Temirov, R.; Jelínek, P. *Phys. Rev. B: Condens. Matter Mater. Phys.* **2014**, *90*, 085421.
(25) Peng, J. B.; Guo, J.; Hapala, P.; Cao, D. Y.; Ma, R. Z.; Cheng, B. W.; Xu, L. M.; Ondráček, M.; Jelínek, P.; Wang, E. G.; Jiang, Y. *Nat. Commun.* **2018**, *9*, 112.
(26) Hapala, P.; Temirov, R.; Tautz, F. S.; Jelinek, P. *Phys. Rev. Lett.* **2014**, *113*, 226101.
(27) Sheng, S.; Wu, J.-b.; Cong, X.; Li, W.; Gou, J.; Zhong, Q.; Cheng, P.; Tan, P.-h.; Chen, L.; Wu, K. *Phys. Rev. Lett.* **2017**, *119*, 196803.
(28) Hapala, P.; Svec, M.; Stetsovych, O.; van der Heijden, N. J.; Ondracek, M.; van der Lit, J.; Mutombo, P.; Swart, I.; Jelinek, P. *Nat. Commun.* **2016**, *7*, 11560.
(29) Hamalainen, S. K.; van der Heijden, N.; van der Lit, J.; den Hartog, S.; Liljeroth, P.; Swart, I. *Phys. Rev. Lett.* **2014**, *113*, 186102.
(30) Speiser, E.; Buick, B.; Esser, N.; Richter, W.; Colonna, S.; Cricenti, A.; Ronci, F. *Appl. Phys. Lett.* **2014**, *104*, 161612.

DOI: 10.1021/acs.nanolett.8b00289
Nano Lett. 2018, 18, 2937−2942

(31) Scalise, E.; Houssa, M.; Pourtois, G.; van den Broek, B.; Afanas'ev, V.; Stesmans, A. *Nano Res.* **2013**, *6*, 19−28.
(32) Stockle, R. M.; Suh, Y. D.; Deckert, V.; Zenobi, R. *Chem. Phys. Lett.* **2000**, *318*, 131−136.
(33) Zhang, R.; Zhang, Y.; Dong, Z. C.; Jiang, S.; Zhang, C.; Chen, L. G.; Zhang, L.; Liao, Y.; Aizpurua, J.; Luo, Y.; Yang, J. L.; Hou, J. G. *Nature* **2013**, *498*, 82−6.
(34) Verma, P. *Chem. Rev.* **2017**, *117*, 6447−6466.
(35) Pozzi, E. A.; Goubert, G.; Chiang, N.; Jiang, N.; Chapman, C. T.; McAnally, M. O.; Henry, A. I.; Seideman, T.; Schatz, G. C.; Hersam, M. C.; Duyne, R. P. *Chem. Rev.* **2017**, *117*, 4961−4982.
(36) Deng, H. *Adv. Protein Chem. Struct. Biol.* **2013**, *93*, 153−82.
(37) Ronci, F.; Colonna, S.; Cricenti, A.; De Padova, P.; Ottaviani, C.; Quaresima, C.; Aufray, B.; Le Lay, G. *Phys. Status Solidi C* **2010**, *7*, 2716−2719.
(38) De Padova, P.; Quaresima, C.; Olivieri, B.; Perfetti, P.; Le Lay, G. *J. Phys. D: Appl. Phys.* **2011**, *44*, 312001.
(39) Ding, Y.; Wang, Y. *J. Mater. Chem. C* **2015**, *3*, 11341−11348.

DOI: 10.1021/acs.nanolett.8b00289
Nano Lett. 2018, 18, 2937−2942